Gas-water steady-state relative permeability determination with two approaches; experimental and digital rock analysis, strengths and weaknesses

R. Farokhpoor[1], E. Westphal[1], N. Idowu[1], P.E. Øren[1], B. Fletcher[2]
[1]FEI Oil and Gas, [2]BG Group, Reading, UK

This paper was prepared for presentation at the International Symposium of the Society of Core Analysts held in Snowmass, Colorado, USA, 21-26 August 2016

ABSTRACT

Digital Rock Analysis (DRA) or pore-scale imaging and modelling have developed significantly in the last decade with the emphasis changing from phenomenological research towards quantitative modelling. The evolution towards more predictive modelling raises questions about the reliability of DRA derived properties compared to experimentally measured data, especially for multiphase flow.

In this work, we compare gas-water relative permeability functions obtained from experimental measurements with those derived from DRA. The steady state tests were performed on single plugs with in-situ saturation monitoring. The experiments showed strong non-uniformity in saturation profiles along the plugs and a numerical approach is used to correct for this artefact.

3D X-ray micro-computed tomography (micro-CT) images of the three sandstone plugs and representative sub-plugs were acquired along with Backscattered Scanning Electron Microscopy (BSEM) images of 2D sections. 3D pore networks were extracted from the sub-plug and process-based models (PBM). Gas-water primary drainage and water-gas imbibition relative permeability curves were calculated on the different networks using a pore network model simulator. The DRA derived relative permeability function displays a large degree of similarity with the experimentally measured one. Comparison of fractional flow curves between the experimental (before bump) and DRA computed results shows a difference of 1.0 to 4.0 saturation units for recovery at breakthrough, suggesting that the observed discrepancies in relative permeability have little implications for practical applications.

INTRODUCTION

Accurate determination of relative permeability is essential in estimating producible reserves and ultimate recovery in reservoir models. Laboratory measurements commonly use flow rates higher than those characteristic of flooding processes in the reservoir to overcome discontinuities in capillary pressure at the boundaries of the core plug. Extensive studies have been performed to minimize this artefact during experiments [1,2]. Numerous approaches have been presented for correcting experimental data using numerical methods, semi-analytical approaches and/or inverse modeling [3-5].

Prediction of multiphase flow properties using DRA has evolved significantly in the last decade and it is becoming a predictive tool in the oil industry. It is generally agreed that

for mixed to oil-wet system, DRA cannot reliably predict multiphase flow properties without detailed representation of contact angles, but for strongly water-wet systems (gas-water systems in this work) DRA results should compare favorably with experimental data. Some authors have compared DRA derived imbibition relative permeability with experimental results for clean sandstones and sandpacks [6-11] but further studies are required for more complicated samples.

In this study, we determined imbibition water-gas relative permeability on three sandstone samples with two approaches. Flow simulations were performed on networks which were extracted from a process-based model and on networks which were extracted from the segmented micro-CT images of the sub-plugs. Comparisons of measured steady-state relative permeability data with predicted results on the same samples show good agreement and differences between the values are within an acceptable range.

Laboratory experimental data

Petrophysical properties of the three core plugs with short lithological descriptions are given in Table 1.

Table 1: Petrophysical and lithological properties of the three core plugs

Plug No.	Depth (m)	Porosity (fraction)	Permeability (mD)	Lithological properties
Plug 1	3186.5	0.233	873	Homogeneous, poorly consolidated, weakly sorted medium to coarse grained sand
Plug 2	4460.14	0.173	1.5	Homogeneous, well sorted fine sandstone
Plug 3	2684.84	0.289	2162	Poorly consolidated, coarse grained sand

Imbibition water-gas steady-state relative permeability experiments were performed on the three core plugs in a core analysis laboratory (Figure 1).

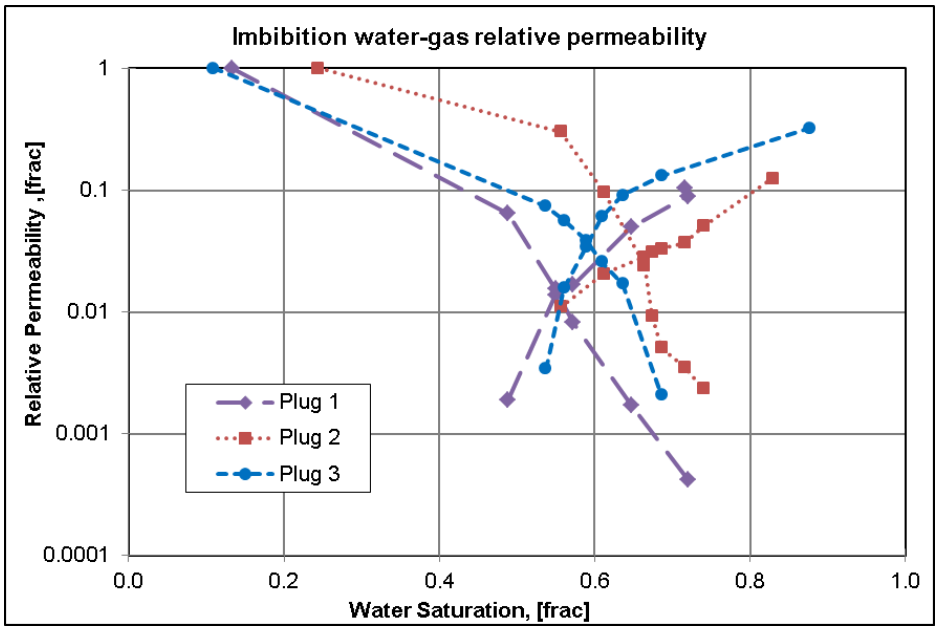

Figure 1: Experimental imbibition water-gas steady-state relative permeability curves

Saturation profiles were mapped during the core plug flooding experiments using an AXRP-300, automated X-Ray relative permeameter. Figure 2 shows that there is a strong non-uniformity in saturation profiles of plugs 1 and 2 while it is less pronounced for plug 3. To correct for this artefact, Sendra simulator was used. The core plug geometry and petrophysical properties were used to build a simple model and to simulate a steady state water-gas imbibition process. The main application is to determine relative permeability from experimental data through an automated history matching of differential pressure (Figure 3-left) and saturation profile. The relative permeability results based on LET [12] correlation are plotted in Figure 3-right.

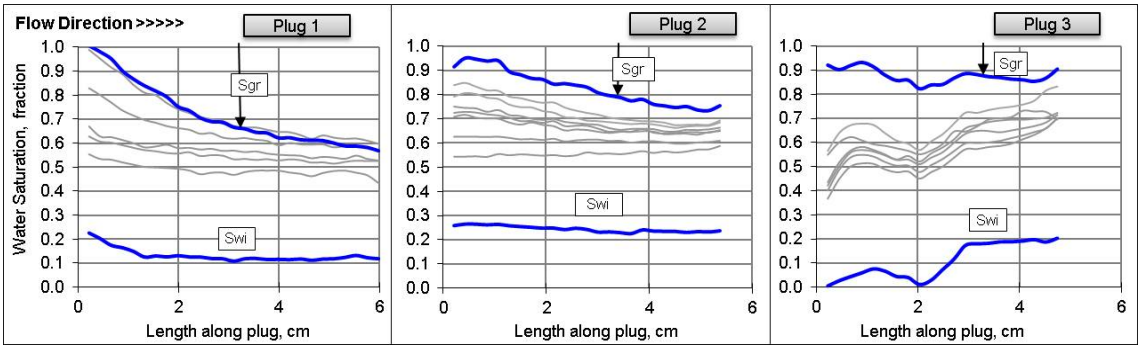

Figure 2: Water saturation profiles along the core plug during flooding experiments

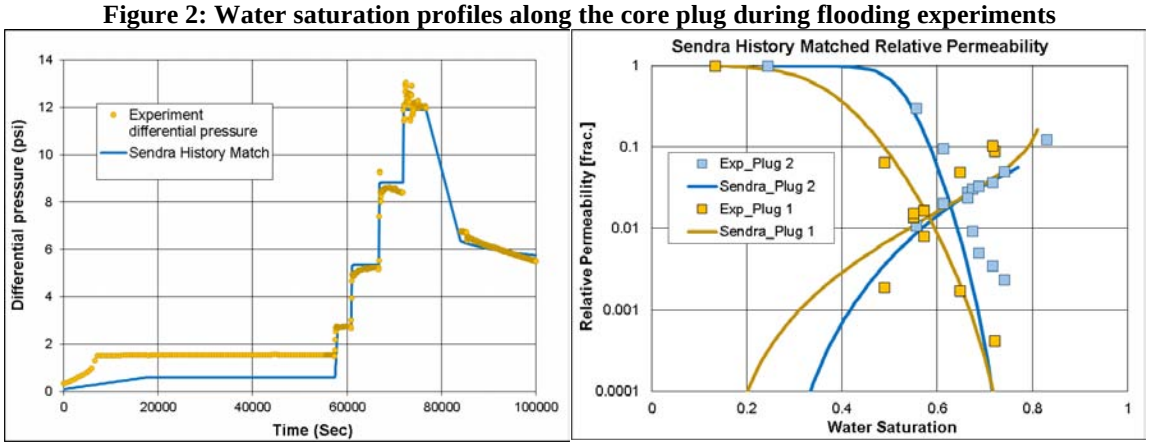

Figure 3: Left) experimental differential pressure and Sendra history matched data for plug 1, Right) comparison of experimental and Sendra relative permeability for plugs 1 and 2

Simulated Sendra results for plug 1 shows that residual gas saturation and water relative permeability are lower compared to the experimental data. In plug 2, the Sendra history matching predicted comparable residual gas saturation and water relative permeability to the experimental data before the bump flood. The main disadvantage of correcting artefact errors using a numerical simulation method is that the results are nonunique and it depends on what correlation has been used.

Digital rock analysis

The workflow used for digital rock analysis can be summarized with the following steps:

1. Overview micro-CT scans of the received core plugs (19µm/voxel)

2. Thin section preparation from a trim end of the core plug and BSEM imaging at multiple scales
3. Image analysis to obtain input data for process-based modelling.
4. PBM construction (capturing relevant rock types).
5. Drilling of a sub-plug (2-5 mm in diameter and 1-2 cm long)
6. Scanning sub-plug by micro-CT at highest possible resolution (1-5 µm/voxel)
7. Processing and generation of rock models from the scanned images
8. Calculation of petrophysical properties (ø, K_{abs}).
9. Extraction of pore network representations from PBM and sub-plug 3D image.
10. Simulation of multiphase flow properties for gas-water system

The workflow is illustrated in Figure 4.

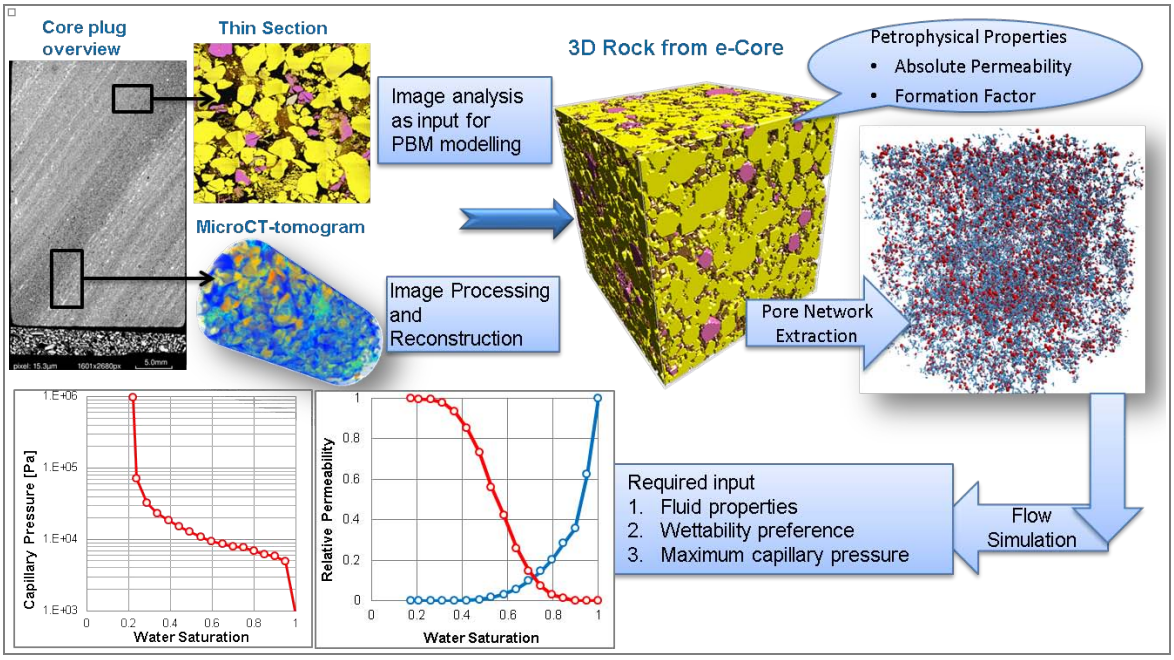

Figure 4: Schematic view of workflow

Imaging

Core plugs of 1.5 inch diameter were scanned on a high resolution micro-CT at 19µm per voxel. The purpose was to:

1. Identify rock types and characterise their distribution and volumes within the core plugs.
2. Select locations for cutting sections through the core plug. Thin sections were prepared and BSEM images were acquired (see Figure 5). These images were used to obtain detailed information on mineralogy, grain size, shape and sorting, pore sizes and any type of clay and cementing minerals.
3. Select location for coring a sub-plug with an attempt to capture a representative elementary volume (REV) from each core plug. Micro-CT scanning of the sub-plugs was carried out on a high-resolution scanner, FEI HeliScan (see Figure 5).

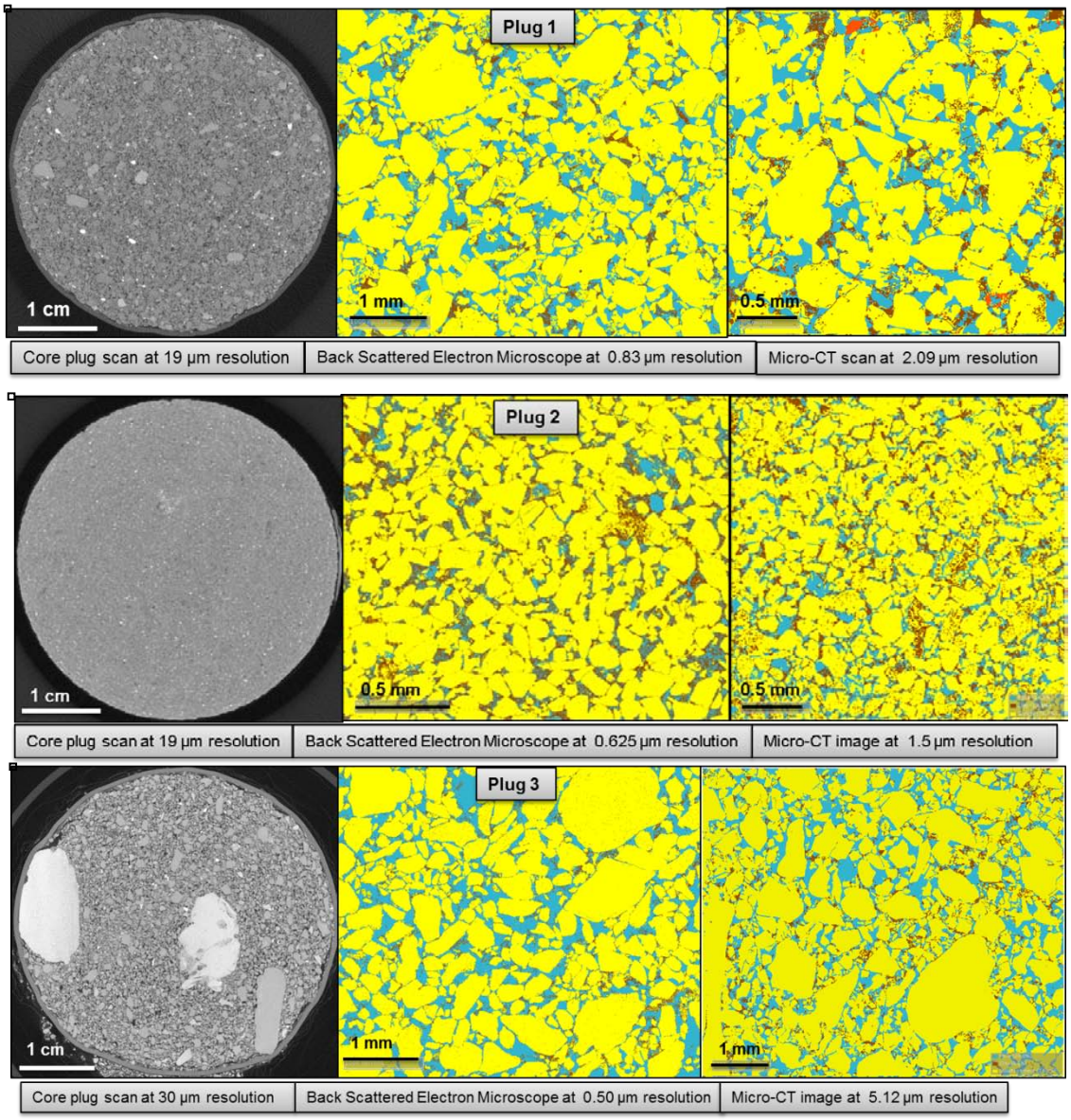

Figure 5: Images of; the core plugs from micro-CT (left), the trim end from BSEM after segmentation (centre), and the sub-plugs from micro-CT. (Yellow color is quartz; orange is feldspar, brown is clay and blue is pore)

Modelling

The BSEM images of the thin section of the core plugs were segmented to produce ternary images of pores; micro-porous phase (clay) and matrix. The ratio of the number of pixels in each threshold bin to the total number of pixels in the image is an estimate for the fraction of the mineral in the rock. For each core plug, one PBM was generated, representing the rock type (RT1) observed in the trim end. For each sample, the proportion of intergranular and micro-porosity, clay content and PBM size and resolution and sub-plug image resolution are given in Table 2.

Table 2: Intergranular and micro-porosity and models size and resolution

Sample	Intergranular porosity (frac)	Micro-porosity (frac)	Clay (%)	PBM size (µm)	PBM resolution (µm)	Sub-plug resolution (µm)
Plug 1	0.206	0.039	6.5	1800	1.0	2.09
Plug 2	0.092	0.080	15.8	720	0.4	1.5
Plug 3	0.248	0.025	6.0	2520	1.4	5.12

Pore-scale resolution 3D models were constructed by PBM, based on the information extracted from the BSEM images. The algorithms applied for the construction of numerical 3D reservoir rock models are based on simulation of the geological processes by which the rock was formed: sedimentation, compaction, and diagenesis [13]. There are several options to place the clay regarding distribution and shape. It can vary from pore lining clay (as often observed in these samples) to more clustered pore-filling clay and to clay from feldspar dissolution. The resulting 3D models are quality checked both visually and statistically against the BSEM images. Figure 6 shows a 3D view of the cubic PBMs for all three plugs.

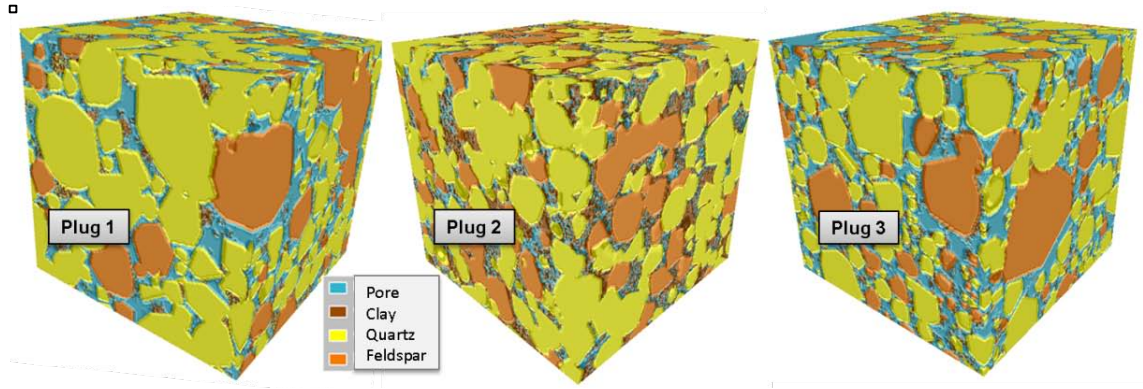

Figure 6: 3D image of process based model for each of the three plugs

The 3D micro-CT scans of the core plug were used to visualize the heterogenity and to select the proper location for one or more subplugs. Micro-CT scan of all three plugs show that one sub-plug is enough to capture the heterogeneity of the plug. To find an REV size for the sub-plug, both pore throat and grain size distribution were considered. BSEM images of the trim ends give useful information about grain size distribution. The minimum diameter for sub-plug is bigger than 15 times the size of the largest grain observed in BSEM. Pore throat size distribution from MICP experiment (if it is available) shows what image resolution is required to be able to capture pore scale phenomenas. For plugs wih smaller pore throat radii, micro-CT scans require higher resolution thus smaller sub-plug is needed (like plug 2).

The micro-CT images of the sub-plugs were segmented according to X-ray attenuation of involved minerals to obtain porosity, micro-porous phase (clay) and matrix. The segmentation was supported by morphological observation. The size of most clay minerals is below the resolution of the images and in most cases it introduces an artefact. Figure 7 shows a 3D view of the micro-CT scans of the sub-plugs and the image dimensions.

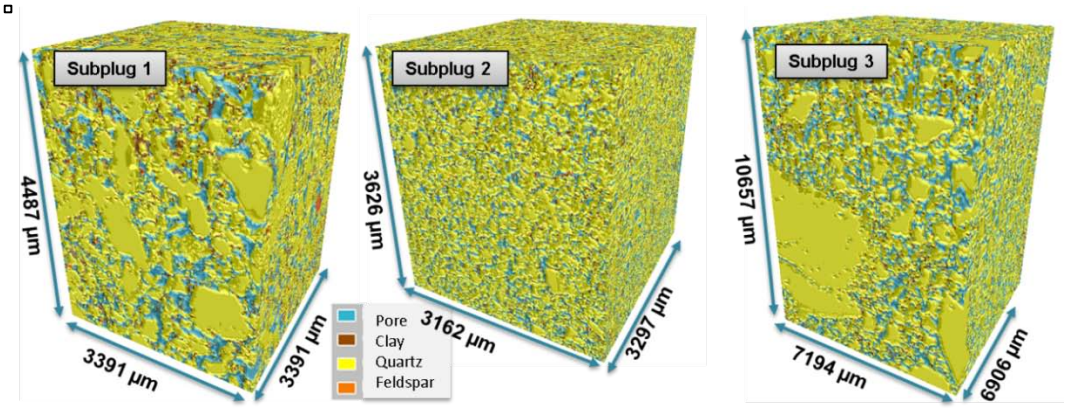

Figure 7: 3D view of sub-plug micro-CT scans

Flow simulation

To perform multiphase flow simulations, the pore space of the reconstructed models is transformed into simplified pore networks, which are used directly as inputs to a network model. Petrophysical properties were calculated for each of the pore scale models, followed by the extraction of their respective pore networks.

The intergranular porosity is given by resolved pores with sizes greater than or equal to the image resolution. The total porosity is the summation of intergranular porosity and sub-resolution porosity (i.e. 0.5-0.6 times the percentage of clay in the rock model). A Lattice-Boltzmann method is applied to solve Stokes' equation in the uniform grid model with maximum 50000 iterations and convergence criteria of 0.005. Flow is driven by a constant pressure gradient through the model. Permeability is calculated with a fluid that does not interact with the rock matrix.

For all samples, calculated porosity is similar to helium porosity and calculated absolute permeability is comparable with Klinkenberg corrected air permeability (see Table 3).

Table 3: Experimental and DRA calculated petrophysical properties

Sample	Helium porosity, (frac)	DRA porosity, (frac)	Klinkenberg permeability, mD	DRA permeability, mD
Plug 1	0.233	0.245	873	1070
Plug 2	0.173	0.172	1.5	0.82
Plug 3	0.289	0.273	2162	1566

The extracted pore networks were used for the simulation of two-phase fluid flow and the calculation of relative permeabilities and capillary pressure curves. The following flow simulations were performed:

- Water-gas primary drainage to initial water saturation (Swi), which is constrained by a maximum capillary pressure of 12.6 bar.
- Water-gas imbibition to residual gas saturation (Sgrw).

The waterflooding process was simulated by assuming the system is strongly water-wet, water index=1.0. The advancing contact angle for water phase was assumed 10-35°.

In all simulations, it is assumed that capillary forces dominate (Nca < 1.0E-6). A detailed account of the methods used for multi-phase flow simulation is given in [14]. Fluid

injection is simulated from one side of the model (usually the x-direction). Thus, the entry pressure is a function of the pore sizes present at the inlet.

Results

Plug 1 is moderately homogeneous and poorly consolidated. Simulated capillary pressure for plug 1 based on the sub-plug and PBM is compared with experimental MICP for a quality control check in Figure 8-left. Capillary pressure corresponding to 2.09 µm resolution in sub-plug is 51675 (Pa) at Sw=0.25. For Sw greater than 0.25, capillary pressure based on the sub-plug is in excellent agreement with the MICP and very good for the PBM (see Figure 8-left). For Sw less than 0.25, there is an insufficient resolution to resolve pores invaded by mercury.

Water-gas imbibition relative permeability simulation results for the PBM and sub-plug are compared with steady state experiments in Figure 9. Simulated water relative permeability for the sub-plug is similar to the steady state experiment but there is a big discrepency in the gas relative permeability.

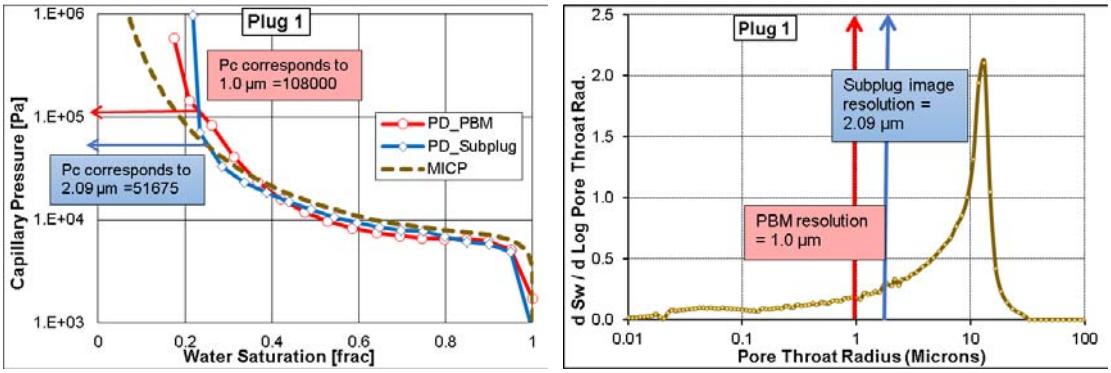

Figure 8: left) Comparison of experimental MICP data with simulated capillary pressure for the PBM and sub-plug, right) pore size distribution from MICP experiment

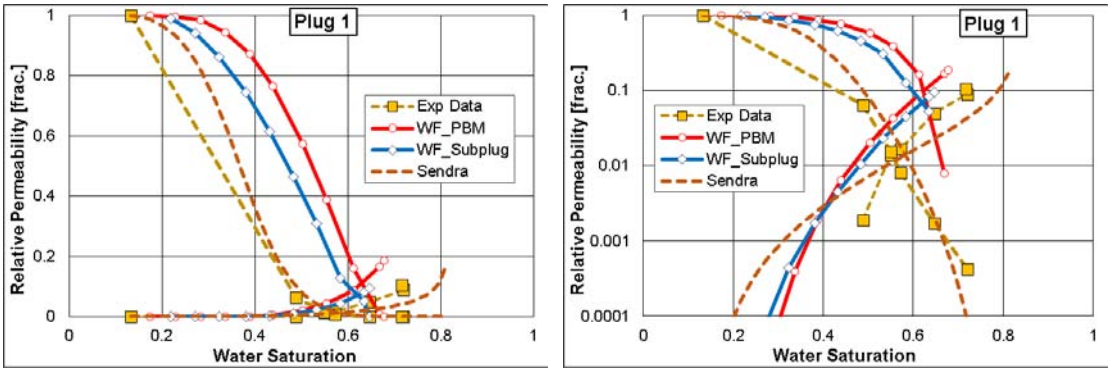

Figure 9: Imbibition water-gas relative permeability curves for the PBM, sub-plug, experimental and Sendra simulation for plug 1

Table 4: Two phase flow results for plug 1

Parameter	Experiment after bump	Experiment before bump	Sendra	PBM	Sub-plug
Swi	0.13	0.13	0.13	0.17	0.21
Sgrw	0.28	0.28	0.19	0.32	0.35
Krw at Sgr	0.105	0.090	0.165	0.187	0.095

Unlike plugs 1 and 3, plug 2 is tight with well sorted, fine grains and is clay rich. The porosity of the plug is 0.17 and almost half of it is micro-porosity (0.08). Experimental MICP pore throat size distribution shows the pore throats are smaller than 1 μm. segmentation of the micro-CT image of the sub-plug (1.5 μm resolution), resulted in a high degree of uncertainity for distinguishing between pores and micro-porous clay patches. As shown in Figure 10, the simulated capillary pressure for the sub-plug is much lower than the experimental MICP while capillary pressure based on the PBM is in excellent agreement with the MICP.

The initial water saturation in the sub-plug simulation is very high, Swi=0.48, and so there is no basis to compare simulated gas-water relative permeability from the sub-plug with the experiment. However, simulated gas and water relative permeability curves and residual gas saturation in the PBM are comparable with the steady state experiment before the bump (see Figure 11).

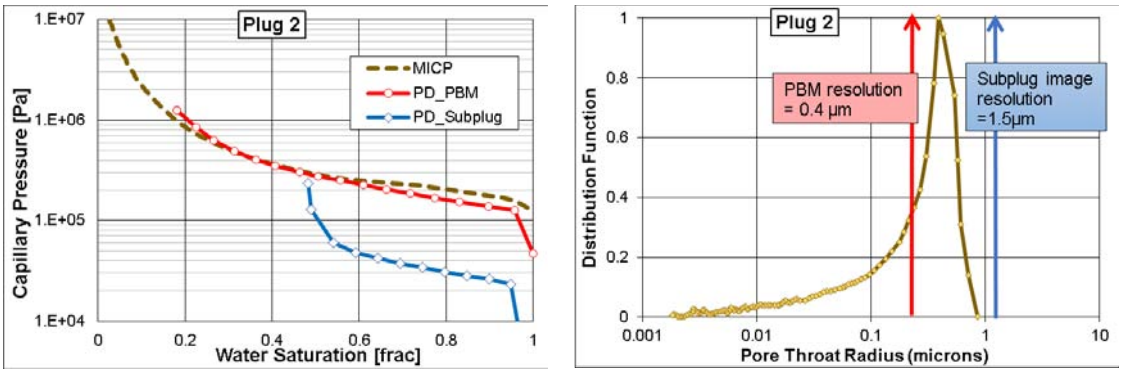

Figure 10: left) Comparison of experimental MICP data with simulated capillary pressure for the PBM and sub-plug, right) pore size distribution from MICP experiment

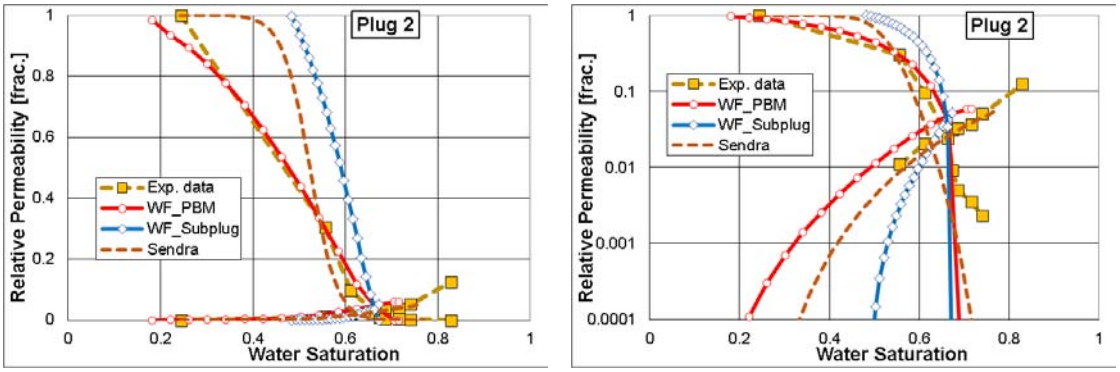

Figure 11: Imbibition water-gas relative permeability curves for the PBM, sub-plug, experimental and Sendra simulation for plug 2

Table 5: Two phase flow results for plug 2

Parameter	Experiment after bump	Experiment before bump	Sendra	PBM	Sub-plug
Swi	0.24	0.24	0.24	0.18	0.48
Sgrw	0.17	0.26	0.23	0.28	0.33
Krw at Sgr	0.125	0.051	0.056	0.059	0.052

Plug 3 is an unconsolidated sandstone and the most porous and permeable sample. Due to the coarseness of the grains, it is difficult to find a REV for a sub-plug. To capture different features, a bigger sub-plug was required compared to the other two samples (see Figure 7). For the bigger sub-plug, the resolution of the micro-CT image is lower, 5.12 µm, thus it is not possible to capture the pores smaller than 5.12 µm. As shown in Figure 12, simulated capillary pressure based on the sub-plug is lower than experimental MICP, especially at lower water saturation. By contrast the PBM simulated capillary pressure is very similar to MICP. Simulated gas and water relative permeability and residual gas saturation based on the PBM is comparable with the steady state experiment before flooding the core plug with high flow rate (see Figure 13).

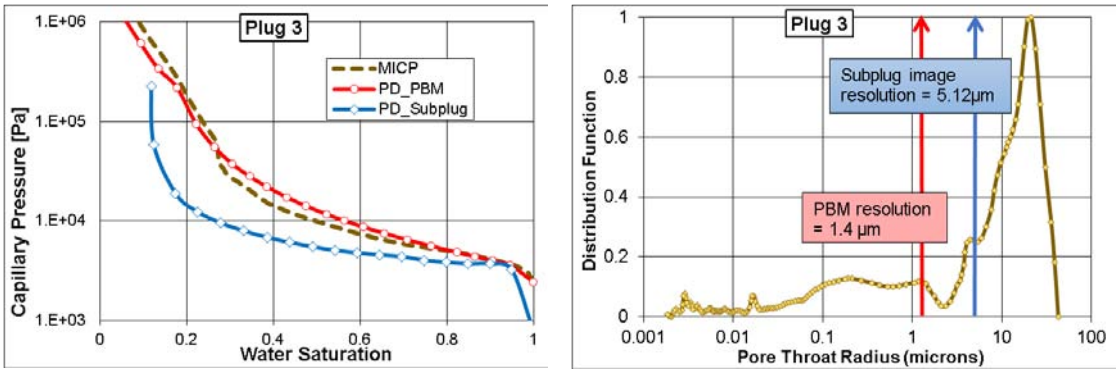

Figure 12: left) Comparison of experimental MICP data with simulated capillary pressure for the PBM and sub-plug, right) pore size distribution from MICP experiment for plug 3

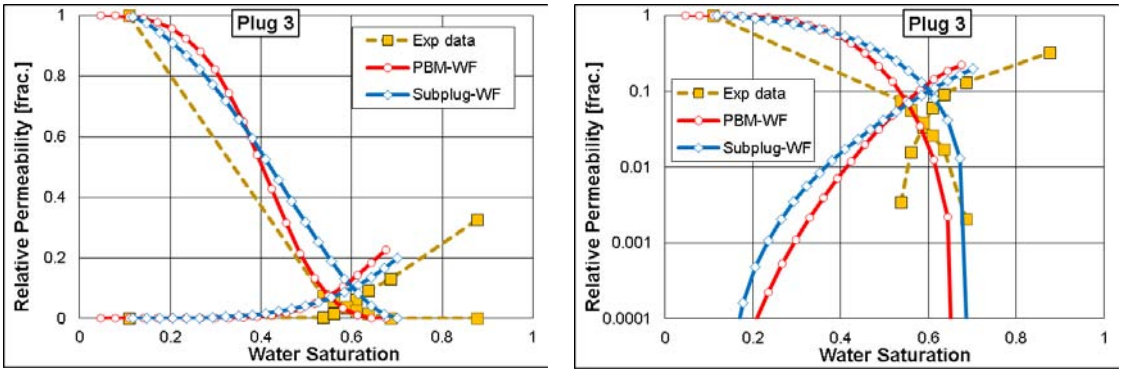

Figure 13: Imbibition water-gas relative permeability curves for the PBM, sub-plug and experiment

Table 6: Two-phase flow results for plug 3

Parameter	Experiment after bump	Experiment before bump	PBM	Sub-plug
Swi	0.11	0.11	0.05	0.12
Sgrw	0.12	0.31	0.32	0.30
Krw at Sgr	0.325	0.131	0.226	0.198

Discussion of Results

For plug 1, the DRA relative permeability on both the sub-plug and PBM show a large degree of similarity with the experimental relative permeability. For plugs 2 and 3, the DRA relative permeability based on the PBM is in good agreement with that from the steady state experiment.

Comparisons of fractional flow curves of experimental and simulated PBM results presented in Figure 14 show differences that range from 1 to 4 saturation unit for recovery at breakthrough (before bump in the experiment). This range is acceptable considering the fact that the initial water saturations are different in the simulations and experiments. With respect to the gas relative permeability, however, there is a big discrepancy in the measured and simulated data. This discrepancy may be due to the fact that there is a suppression of gas connectivity/conductivity due to non-uniform saturation profiles (lower gas saturation at the inlet) shown in Figure 2.

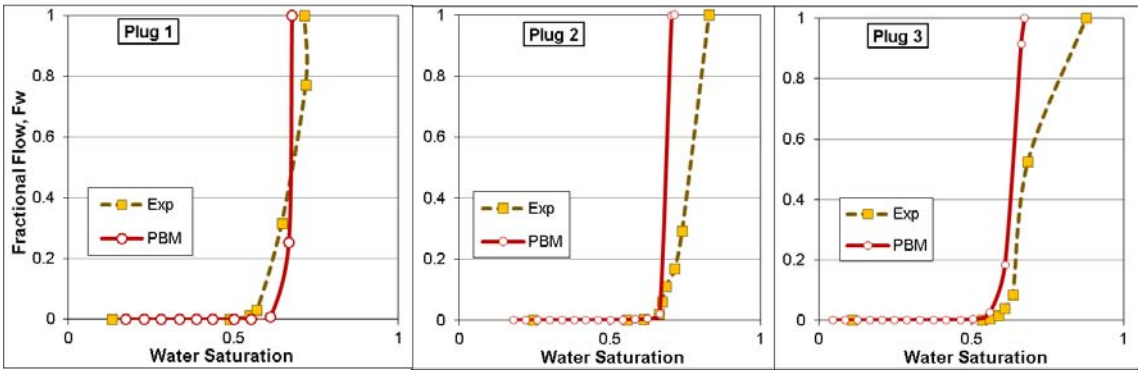

Figure 14: Fractional flow curves for experiment and PBM simulation for all plugs

CONCLUSION

Three sandstone samples were tested to compare gas-water relative permeability data from two different approaches: steady state experiment and DRA. The DRA simulations were performed on the micro-CT image of the sub-plug and on a process-based model. Comparison of fractional flow curves from experiment and DRA shows a good agreement in recovery after breakthrough. The discrepancy in water relative permeability is within an acceptable range and with one exception, the same trend was observed for gas relative permeability.

Non-uniform water saturation along the core plug displays artefacts (disequilibria effects or capillary-end effects) in the coreflood experiments, which can significantly influence the computation of end-point relative permeabilities and saturation. Numerical approaches (like Sendra in this work) can be useful to correct for this artefact, but it doesn't account for the core heterogeneity and also it doesn't give a unique result.

In conclusion, there are complications and uncertainties in both experimental and simulation approaches, but the observed discrepancies have little implications for practical applications.

Significant improvements have been made in sample handling and thin section preparation, the micro-CT imaging technology and image processing tools since this work was completed in 2015.

ACKNOWLEDGEMENTS

We would like to acknowledge BG UK for providing experimental data and allowing the publishing of the results.

REFERENCES

[1] A. L. Chen and A. C. Wood, "Rate effects on water-oil relative permeability," Society of Core Analysts, 2001, SCA2001-19.

[2] R. Gupta and D. Maloney, "Application of the intercept method to correct steady-state relative permeability for capillary-end-effect," Society of Core Analysts, 2015, SCA2015-01.

[3] S. Qadeer, K. Dehghani, D. O. Ogbe and R. D. Ostermann, "Correcting oil/water relative permeability data for capillary end effect in displacement experiments," Society of Petroleum Engineers, 1988, 7423-MS.

[4] F. Hussain, Y. Cinar and P. Bedrikovetsky, "A semi-analytical model for two phase immiscible flow in porous media honoring capillary pressure," Transport in Porous Media, 2012, vol. 92, no. 1, pp. 187-212.

[5] M. H. Krause, J. C. Perrin and S. M. Benson, "Modeling permeability distributions in a sandstone core for history matching coreflood experiments.," Society of Petroleum Engineers, 2009, SPE 126340.

[6] M. Piri and M. Blunt, "Three-dimensional mixed-wet random pore-scale network modeling of two- and three-phase flow in porous media. II. Results," PHYSICAL REVIEW E 71, 2005, vol. 026302, pp. 1-11.

[7] M. Blunta, B. Bijeljica, H. Dongb, O. Gharbia, S. Iglauerc, P. Mostaghimia, A. Palusznya and C. Pentlanda, "Pore-scale imaging and modelling," Advances in Water Resources, 2013, vol. 51, p. 197–216.

[8] B. Raeesi, N. Morrow and G. Mason, "Pore network modelling of experimental pressure hysteresis relationships," Society of Core Analysts, 2013, SCA2013-15.

[9] A. Aghaei and M. Piri, "Direct pore-to-core up-scaling of displacement processes: Dynamic pore network modeling and experimentation," Journal of Hydrology, 2015, vol. 522, p. 488–509.

[10] C. H. Pentland, Y. Y. Tanino, S. Iglauer and M. Blunt, "Capillary trapping in water-wet sandstones: coreflooding experiments and pore-network modeling," Society of Petroleum Engineers , 2010, SPE 133798.

[11] P. Valvatne and M. Blun, "Predictive pore-scale modeling of two-phase flow in mixed wet media," Water Resources Research, 2004, vol. 40, pp. W07406-1-21.

[12] F. Lomeland, E. Ebeltoft and T. Hammervold , "A new versatile relative permeability correlation," Society of Core Analysts, 2005, SCA2005-32.

[13] P.-E. Øren and S. Bakke, "Process based reconstruction of sandstones and prediction of transport properties," Transport in Porous Media, 2002, pp. 311-343.

[14] P.-E. Øren, S. Bakke and O. J. Arntzen, "Extending predictive capabilities to network," SPE Journal, 1998, pp. Vol 3, Issue 4.